The 8th European Congress on Computational Methods in Applied Sciences and Engineering
ECCOMAS Congress 2022
5–9 June 2022, Oslo, Norway

WAVE BASED METHOD FOR 2D UNSATURATED POROELASTIC SOIL UNDER HARMONIC LOADING

M. Lainer and G. Müller

Chair of Structural Mechanics, TUM School of Engineering and Design
Technical University of Munich
Arcisstraße 21, 80333 Munich, Germany
e-mail: mirjam.lainer@tum.de, gerhard.mueller@tum.de
web page: www.cee.ed.tum.de/bm

Key words: Wave Based Method, Unsaturated Soils, Poroelasticity

Abstract. The Wave Based Method (WBM), which describes field variables of a boundary value problem with weighted wave functions, is used to model a layered halfspace under harmonic loading. This 2D soil structure is investigated for partially saturated layers. According to the Berryman-Thigpen-Chin model (BTC model) the capillary effects between the water and air phases enclosed by pores are negligibly small for elastic waves in the low frequency range. The mixture of water and air is treated as one fluid, for which the material parameters used in Biot's theory for fully saturated poroelastic structures have to be computed. Within this work, the BTC model is applied to describe soil layers within a halfspace, which are not perfectly dry or fully saturated. It is presented how the degree of saturation within a partially saturated soil layer affects the system's response.

1 INTRODUCTION

Considering soil as a poroelastic structure, it is necessary to specify the fluid or respectively the fluid composition, which is enclosed by a solid skeleton. The Biot theory [1, 2] permits to describe the coupling effect between a single fluid, for example water, and the surrounding structure. In the case of a 2D problem, the displacement variables consist of solid phase displacements $\mathbf{u}^s$ and seepage field components $\mathbf{U} = n^f(\mathbf{u}^f - \mathbf{u}^s)$. The latter also depends on the global fluid deformations $\mathbf{u}^f$ and the porosity n^f. The system's response is expressed as a superposition of two irrotational potentials $\Phi_{p_{1/2}}$ and one solenoidal potential Ψ_s.

Biot's theory is extended by considering an additional air content within the pores of the soil structure. In order to describe the interaction between the air phase with the water phase and the surrounding skeleton, different mathematical models have been derived. These describe the dynamic response of an unsaturated structure by considering three compressional waves and one shear wave. In particular, the description of the interaction between two immiscible fluids in the pores is typically challenging, as influences from drag and capillary forces need to be considered. In the case of a water saturated soil domain, already a small degree of air saturation may change the dynamic system response significantly, as shown by Murphy [3]. This paper presents results of resonant bar tests for probes with Massilon sandstone and Vycor porous glass under harmonic loading, whose pores are filled with water and air. Within these experiments the velocity and

the attenuation of the first compressional wave and the shear wave were measured for different excitation frequencies and degrees of saturation. It was possible to validate the measured wave velocities. However, for the attenuation measurements it is stressed out that no appropriate model could be applied to reproduce the experiment results.

The published experiment data by Murphy has been used in further investigations by other authors in order to validate their models for partially saturated poroelastic continua. Berryman, Thigpen and Chin (BTC model) have introduced in their publication [4] two models to cope with segregated fluids (water-oil) and mixed fluids (water-air) to elaborate the attenuation within an unsaturated medium. It is assumed that low frequency interactions due capillary pressure effects can be neglected. The mathematical model consists two compressional waves and one shear wave for the 2D case. This low frequency region is delimited by a critical frequency with magnitudes from 10^3 to 10^6 Hz [5]. In a similar approach, Biot's theory was extended for a small gas ratio by considering the specific construction of the air bubbles [6]. This model was then applied to the numerical investigation of soil domains with dry, saturated or unsaturated layers under a harmonic or transient loading [7].

Another approach is based on the continuum theory of mixtures with interfaces [8, 9], which considers interaction processes due to drag and capillary forces between two phases. This mathematical model has successfully been implemented within a hybrid Trefftz finite element approach, modeling the poroelastic behavior of a partially saturated halfspace for transient loading [10,11]. Within further investigations, additional inertial coupling forces between two immiscible fluids were involved into a mathematical model [12, 13].

The cited researches motivated to extend the Wave Based Method (WBM) by an unsaturated poroelastic element according to the BTC model and to investigate the influence of partial saturation on the dynamic response of a layered halfspace. The WBM has firstly been introduced by [14] to analyze vibro-acoustic problems. During the last two decades it has been applied to further dynamic problem descriptions such as for example coupled vibro-acoustic structures and poroelastic media [15]. In general, the WBM uses weighted wave functions, which fulfill the underlying differential equations of a boundary value problem, in order to describe the desired field variables. The accuracy of the WBM is strongly connected to the ratio between the prevailing excitation frequency and the geometrical size of the considered system, which is expressed by a truncation factor T. This makes it possible to transfer the WBM from the field of vibro-acoustic problems to soil domains, without increasing the number of unknowns significantly. Typically, vibro-acoustic structures deal with small or mid-sized domains for a medium frequency range, while soil dynamic descriptions are usually characterized by relatively large domains and low excitation frequencies. This leads to similar truncation factors for vibro-acoustic and soil dynamic problem descriptions.

In the following part of this paper, the BTC model is introduced and it is presented how it is embedded within the Biot theory. Afterwards the main characteristics of the WBM are depicted, especially its application to poroelastic structures. Finally, a two-layered halfspace with dry, saturated and unsaturated soil layers is modeled and analyzed for a harmonic loading with different excitation frequencies. The chosen problem description is taken from [16], who investigated i.a. the dynamic behavior of Molsand soil with a dry elastodynamic layer placed on a saturated poroelastic subdomain. Selected results are compared with this reference data in order to assess the accuracy of the WBM.

2 DESCRIPTION OF AN UNSATURATED POROELASTIC STRUCTURE

For a poroelastic structure filled with water and air, the two fluid phases are described as one mixed fluid according to the BTC model. For a 2D continuum, the displacement field consists of solid phase displacements $\mathbf{u}^s = [u_x, u_y]^T$ and a seepage field $\mathbf{U} = [U_x, U_y]^T$. The latter describes the relative displacements between the mixed fluid and the solid skeleton related to the total volume of the structure by the porosity n^f: $\mathbf{U} = n^f(\mathbf{u}^f - \mathbf{u}^s)$. It consists of the contributions from the water phase $\mathbf{U}_1$ and the air phase $\mathbf{U}_2$. In the following compatibility condition, ζ expresses the change of the mixed fluid content or respectively the amount of fluid flowing out of the pores.

$$\begin{pmatrix} \varepsilon_{xx} \\ \varepsilon_{yy} \\ \gamma_{xy} \\ \zeta \end{pmatrix} = \begin{bmatrix} \frac{\partial}{\partial x} & 0 & 0 & 0 \\ 0 & \frac{\partial}{\partial y} & 0 & 0 \\ \frac{\partial}{\partial y} & \frac{\partial}{\partial x} & 0 & 0 \\ 0 & 0 & \frac{\partial}{\partial x} & \frac{\partial}{\partial y} \end{bmatrix} \begin{pmatrix} u_x \\ u_y \\ U_x \\ U_y \end{pmatrix} \tag{1}$$

The formulation of the constitutive equations is based on the plane strain state and involves the total fluid stresses σ_f due a mixed water-air-phase, which is leaving or flowing into the pores. The parameters λ and μ are the first and second Lamé coefficients, addressed to the solid skeleton. These are based on the complex E-modulus $E(1 + i\eta)$, with the Young's modulus E for drained rock and the loss factor η. The first and second Biot coefficients are expressed as α and M and strongly depend on the bulk modulus K_f of the mixed fluid.

$$\begin{pmatrix} \sigma_{xx} \\ \sigma_{yy} \\ \tau_{xy} \\ \sigma_f \end{pmatrix} = \begin{bmatrix} \lambda + 2\mu + \alpha^2 M & \lambda + \alpha^2 M & 0 & \alpha M \\ \lambda + \alpha^2 M & \lambda + 2\mu + \alpha^2 M & 0 & \alpha M \\ 0 & 0 & \mu & 0 \\ \alpha M & \alpha M & 0 & M \end{bmatrix} \begin{pmatrix} \varepsilon_{xx} \\ \varepsilon_{yy} \\ \gamma_{xy} \\ \zeta \end{pmatrix} \tag{2}$$

In compliance with Biot's theory, the deformation fields for the solid matrix and the mixed fluid seepage field correspond to a superposition of two irrotational potentials $\Phi_{p_{1/2}}$ and one solenoidal potential Φ_s.

$$\mathbf{u}^s = \boldsymbol{\nabla}\Phi_{p_1} + \boldsymbol{\nabla}\Phi_{p_2} + \widetilde{\boldsymbol{\nabla}}\Psi_s \tag{3}$$

$$\mathbf{U} = \gamma_{p_1}\boldsymbol{\nabla}\Phi_{p_1} + \gamma_{p_2}\boldsymbol{\nabla}\Phi_{p_2} + \gamma_s\widetilde{\boldsymbol{\nabla}}\Psi_s \tag{4}$$

$$\text{with } \boldsymbol{\nabla} = \left[\frac{\partial}{\partial x}, \frac{\partial}{\partial y}\right]^T, \ \widetilde{\boldsymbol{\nabla}} = \left[\frac{\partial}{\partial y}, -\frac{\partial}{\partial x}\right]^T$$

The values γ_{p_1}, γ_{p_2} and γ_s are derived within a decoupling procedure of the equations of propagation, as shown in [1]. These parameters are necessary to evaluate the wave numbers for the first and second P-wave and the S-wave. The coupling parameter ρ_{f2} describes the interaction between the mixed fluid phase and the solid matrix. It consists of a real part, related to the mixed fluid density and the pore volume, as well as an imaginary part, which is characterized by a dissipation factor and its frequency dependency.

$$k_{p_{1/2}} = \sqrt{\frac{\rho_f + \gamma_{p_{1/2}}\rho_{f2}}{(\alpha + \gamma_{p_{1/2}})M}} \cdot \omega, \quad k_s = \sqrt{\left(1 + \gamma_s \frac{\rho_f}{\rho}\right)\frac{\rho}{\mu}} \cdot \omega \tag{5}$$

$$\text{with } \rho_{f2} = \frac{\rho_f a}{n^f} - \frac{i\xi}{\omega (n^f)^2}, \quad \xi = \frac{\rho_f \cdot (n^f)^2}{k_c} \cdot 9.81\text{m/s}^2, \quad k_c = \frac{\kappa \cdot \rho_f}{\eta_f} \cdot 9.81\text{m/s}^2$$

To assess the influence of saturation on the dynamic behavior of a soil layer, the numerical examples of this paper deal with Molsand soil. This permits to use reference solutions for selected numerical results. Moreover, it is possible to apply the material parameters for a dry elastodynamic soil structure, a fully saturated domain, or a partially saturated layer according to the BTC model. The necessary model parameters are summarized in Table 1, whereby for the hydraulic conductivity k_c a medium high value is assumed. This permits relative displacements between solid and fluid phase, which do not tend to zero.

Table 1: Material parameters for Molsand soil

Model	Symbol	Value	Definition
Lamé	ρ_s	2650 kg/m^3	density, solid matrix
	n^f	0.388	porosity
	ρ	1621.8 kg/m^3	density, mixture
	$E(1+i\eta)$	$2.98 \cdot 10^8 \cdot (1+i\eta)$ N/m^2	Young's modulus, drained rock
	η	0.05	loss factor, drained rock
	ν	0.333	Poisson's coefficient
Biot	ρ_1	1000 kg/m^3	density, water
	ρ	2009.8 kg/m^3	density, mixture
	K	$5.97 \cdot 10^9$ N/m^2	bulk modulus, mixture
	α	1.0	1st Biot coefficient
	M	$5.67 \cdot 10^9$ N/m^2	2nd Biot coefficient
	k_c*	0.01 m/s	hydraulic conductivity
	a_t	1.0	tortuosity
BTC	S	$[0, 1.0]$	water saturation
	θ_1	$n^f \cdot S$	volume fraction, water
	θ_2	$n^f \cdot (1-S)$	volume fraction, air
	ρ_2	1.1 kg/m^3	density, air
	ρ_f	$(\rho_1 \cdot \theta_1 + \rho_2 \cdot \theta_2)/n^f$	fluid density
	K_1	$2.19996 \cdot 10^9$ N/m^2	bulk modulus, water
	K_2	$1.45 \cdot 10^5$ N/m^2	bulk modulus, air
	K_f	$n^f \cdot (\theta_1/K_1 + \theta_2/K_2)^{-1}$	bulk modulus, mixed fluid
	η_1	$1.0 \cdot 10^{-3}$ Ns/m^2	dynamic viscosity, water
	η_2	$1.8 \cdot 10^{-5}$ Ns/m^2	dynamic viscosity, air
	η_f	$(\theta_1 \cdot \eta_1 + \theta_2 \cdot \eta_2)/n^f$	dynamic viscosity, mixed fluid
	κ	$1.0194 \cdot 10^{-9}$ m^2	intrinsic permeability

* Originally, the hydraulic conductivity for Molsand soil was measured with $k_c = 0.0001$m/s [16].

The BTC model describes the attenuation coefficients for the irrotational potentials and the solenoidal potential as frequency dependent values. These are deduced from the wave numbers $k_\bullet$ for the first and second P-wave and the S-wave, with $\bullet \in \{p_1, p_2, s\}$. In the following equation, the parameter $c_\bullet$ indicates the wave velocity and $1/Q_\bullet$ represents the attenuation coefficient.

$$k_\bullet \cong \frac{\omega}{c_\bullet} \cdot \left(1 + \frac{1i}{Q_\bullet}\right), \text{ with } \omega = 2\pi f \tag{6}$$

The attenuation coefficients $1/Q_{p_1}$ and $1/Q_s$ for Molsand soil and an excitation frequency $f \in \{12.5, 75, 100\}$[Hz] are depicted in Figure 1. These were evaluated for the Lamé equations, the Biot theory and the BTC model with a saturation $S \in [0.01, 1.0]$. The BTC model reveals a maximum attenuation of the first P-wave ($1/Q_{p_1} = 0.15$) for $S = 0.95$ and $f = 75$Hz. For $S > 0.95$, the attenuation coefficient decreases rapidly, which is linked to the bulk modulus of the mixed fluid K_f. Table 1 shows that K_f depends on the bulk moduli of the water and air phase, which are involved into a serial connection procedure. This causes a rapid loss in the attenuation of the first compressional wave for a low air content in the pores. However, for $S = 1.0$ the BTC model delivers the same attenuation coefficient as Biot's theory.

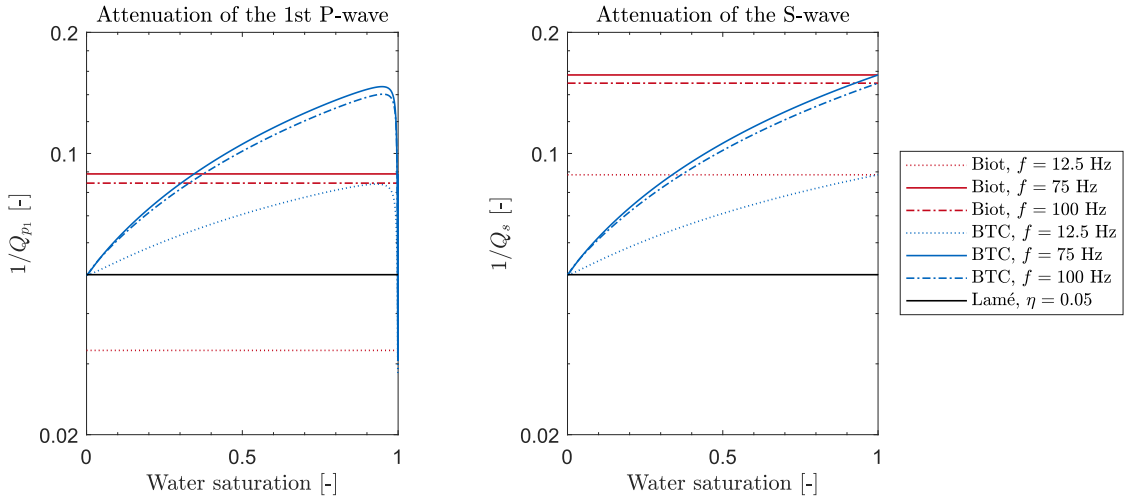

Figure 1: Attenuation coefficients for Molsand soil, evaluated for a dry elastodynamic (Lamé), fully saturated (Biot) and unsaturated material (BTC)

Such a peak cannot be observed for $1/Q_s$, which steadily grows for an increasing S. The attenuation of the S-wave depends on the density of the mixed fluid and rises with the saturation. In contrast to the attenuation coefficient for the first P-wave, it does not depend on compressional deformations in the solid skeleton or within the mixed fluid. For a saturation close to 1.0, the value $1/Q_s$ approaches the attenuation coefficient according to Biot's theory.

Furthermore, Figure 1 illustrates that the values $1/Q_{p_1}$ and $1/Q_s$, which are computed according to the BTC and Biot model, are frequency dependent and may reach an optimum damping state for the system. This optimum damping state is characterized by a critical excitation frequency as shown by [16]. Below this critical frequency, the system tends to a frozen

state, within which the coupling forces between the mixed fluid and the solid matrix prevent relative fluid displacements. For higher frequencies, the coupling forces have less influence and the mixed fluid and the solid skeleton behave more like an uncoupled system. Moreover, the depicted graphs illustrate that the elastodynamic domain according to the Lamé equations does not reveal a damping behavior which is frequency or saturation dependent.

3 CHARACTERISTICS OF THE WAVE BASED METHOD

In order to compute the displacement fields $\mathbf{u}^s$ and $\mathbf{U}$ from the equations (3) and (4), the irrotational potentials $\Phi_{p_{1/2}}$ and the solenoidal potential Ψ_s are approximated by a sum of weighted wave functions. These wave functions fulfill the underlying differential equations and are classified into sets for the first and second P-wave as well as for the S-wave. The wave functions were chosen according to [17] and depend on the wave numbers k_{p_1}, k_{p_2} and k_s, as well as on the geometry of the considered subdomains.

$$\mathbf{u}_h^s \cong \widehat{\mathbf{u}}_h^s = \sum_{i=1}^{n_{p1}} c_{p_1,i} \boldsymbol{\nabla} \Phi_{p_1,i} + \sum_{j=1}^{n_{p2}} c_{p_2,j} \boldsymbol{\nabla} \Phi_{p_2,j} + \sum_{k=1}^{n_s} c_s \widetilde{\boldsymbol{\nabla}} \Psi_{s,k} \tag{7}$$

$$\mathbf{U}_h \cong \widehat{\mathbf{U}}_h = \sum_{i=1}^{n_{p1}} \gamma_{p_1} c_{p_1,i} \boldsymbol{\nabla} \Phi_{p_1,i} + \sum_{j=1}^{n_{p2}} \gamma_{p_2} c_{p_2,j} \boldsymbol{\nabla} \Phi_{p_2,j} + \sum_{k=1}^{n_s} \gamma_s c_{s,k} \widetilde{\boldsymbol{\nabla}} \Psi_{s,k} \tag{8}$$

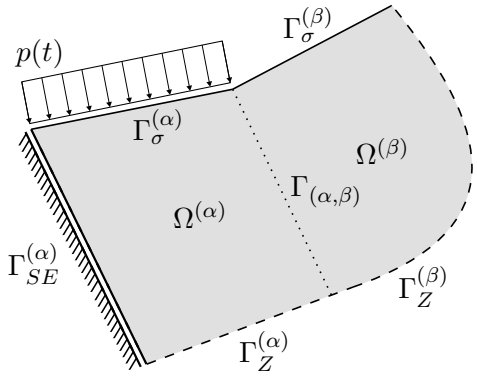

Figure 2: Definition of subdomains and boundaries

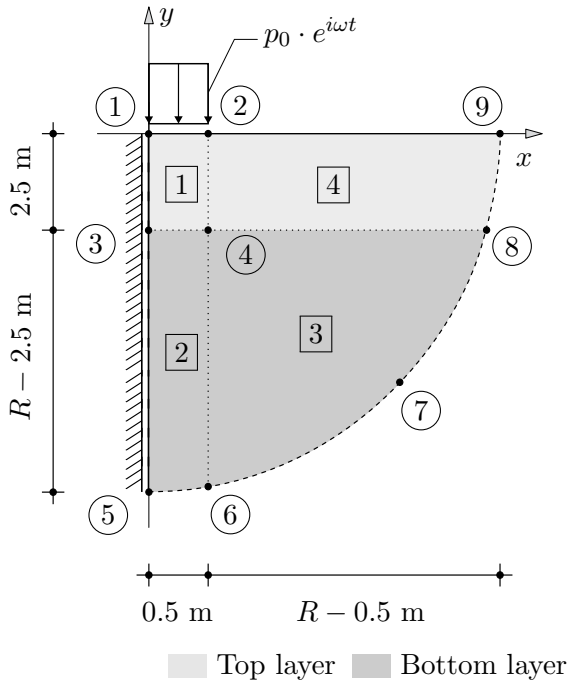

Figure 3: Description of a domain with two layers

The weighting values $c_\bullet$ from the equations (7) and (8) are deduced within a weighted residual Galerkin approach. As the wave functions mostly violate the boundary conditions of a subdomain, residuals are formulated along the edges. Figure 2 gives an overview of possible boundary conditions. These consist of Neumann (Γ_σ), Dirichlet (Γ_u) and mixed (Γ_{SE}) boundary conditions as well as coupling conditions ($\Gamma_{(\alpha,\beta)}$) between two adjoining domains. The formulated residuals are weighted by wave functions and summed up in order to set up a final system of linear equations. Its solution is a vector of unknowns, which contains the weighting values for the predefined wave functions.

4 ANALYSIS OF A HALFSPACE WITH TWO LAYERS

4.1 Definition of the 2D model

Figure 3 depicts a quarter with the radius $R \in \{10 \text{ m}, 20 \text{ m}\}$ and a thickness of 1.0 m in z-direction. This structure describes the reduced model of a symmetrically loaded halfspace. The halfspace is excited by a harmonic loading with the amplitude $p_0 = 1.0$ N/m in vertical direction, which is constantly distributed along a strip with a length of 1.0 m. The first layer has a width of 2.5 m and is modeled by the elements $\boxed{1}$ and $\boxed{4}$. The remaining elements, $\boxed{2}$ and $\boxed{3}$, are used to construct the second layer. Each element is built by four nodes $\textcircled{i}$, with $i \in \{1, 2, 3, 4, 5, 6, 7, 8, 9\}$. The vertical boundaries $\textcircled{1} - \textcircled{3}$ and $\textcircled{3} - \textcircled{5}$ are described by a sliding boundary condition, whereas for the horizontal edges $\textcircled{1} - \textcircled{2}$ and $\textcircled{2} - \textcircled{9}$ Neumann boundary conditions are necessary. The circular edges are modeled with an absorbing boundary condition according to [16], which permits the transmission of normally incident waves (1st and 2nd P-wave, S-wave). Inter-element coupling conditions consider force equilibrium and displacement compatibility between two adjoining elements [17].

Fully saturated domains are modeled by elements, which consider Biot's theory, whereas for partial saturation the BTC model is applied. Dry elastodynamic soil layers are called Lamé elements. In the following, the soil structure is assessed for different types of layering. Table 2 depicts these six models and their layers.

Table 2: Soil models and corresponding layer composition

Soil model	Top layer	Bottom layer
A	dry (Lamé)	full saturation (Biot)
B	dry (Lamé)	partial saturation (BTC)
C	partial saturation (BTC)	full saturation (Biot)
D	dry (Lamé)	dry (Lamé)
E	full saturation (Biot)	full saturation (Biot)

4.2 Mean displacement amplitude for model A

Within the first numerical evaluation, the presented halfspace is modeled with a dry top layer and fully saturated bottom layer. The harmonic loading is applied for different excitation frequencies $f \in \{12.5, 25, 37.5, 50, 62.5, 75, 87.5, 100\}$ [Hz]. For each of them the mean average displacement amplitude $\overline{u}_y$ under the loaded strip is computed.

$$\overline{u}_y = \frac{1}{0.5\ \text{m}} \int_0^{0.5\ \text{m}} |u_y|\, dx \tag{9}$$

The results for the mean displacements in dependency of the excitation frequency are depicted in Figure 4 together with a reference solution by [16] for a spectral element approach. For a radius $R = 10$ m, the WBM approximates the reference solution closely for $f \geq 37.5$ Hz with a deviation between 0.42% (75 Hz) and 3.1% (87.5 Hz). For lower frequencies, the WBM results differ strongly from those with the spectral element method. This probably results from reflections along the circular edges of the halfspace, especially in the upper layer. As the applied absorbing boundary condition only transmits normally incident P- and S-waves, spurious reflections may occur for non-perpendicular wave fronts as well as surface waves. This effect is reduced by increasing the radius of the model. Wave fronts, which reach the circular edges, are more strongly damped and have less influence on the system's response due to spurious reflections. This is illustrated by a red dashed graph in Figure 4, which indicates a better approximation of the reference solution for lower frequencies.

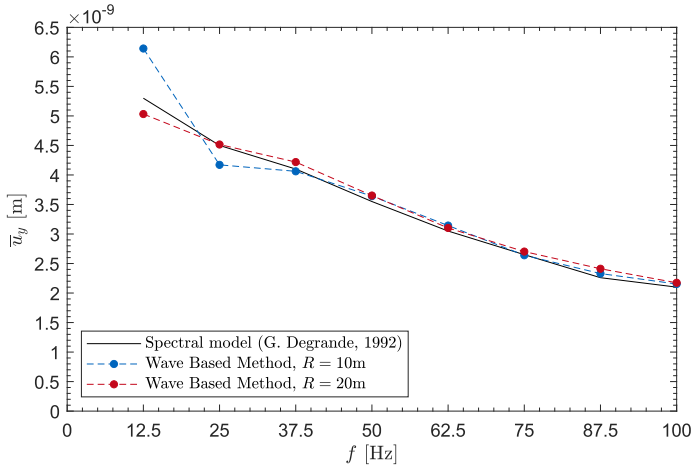

Figure 4: Average displacement amplitude $\overline{u}_y$ for model A

All three graphs in Figure 4 show a slight plateau for an excitation frequency between 25 Hz and 37.5 Hz, which is characteristic for a halfspace with a water table. Regarding this effect, [16] carried out parameter studies to evaluate the influence of the hydraulic conductivity k_c and the excitation frequency. For a very low hydraulic conductivity (e.g. $k_c = 0.0001$ m/s), the bottom layer tends to the state of a frozen mixture, so that there are hardly relative displacements between solid and liquid phase. This causes a significant difference in the impedance between bottom and top layer, which goes along with additional amplifications in the displacement amplitude $\overline{u}_y$. For a higher hydraulic conductivity, relative motions between the solid phase and the enclosed fluid increase and less reflections occur along the transition from the top to the bottom layer. For the presented simulation results, a medium hydraulic conductivity $k_c = 0.01$ m/s was chosen, so that still a slight plateau for $\overline{u}_y$ is visible. Whereas in the case of a very high hydraulic conductivity (e.g. $k_c = 1.0$ m/s) as shown by [16], the displacement

amplitude would decrease steadily for a growing excitation frequency. In the following numerical examples it will be analyzed how the field response of such a layered structure may change, if one of the prescribed layers is not considered to be perfectly dry or fully saturated.

4.3 Mean displacement amplitude for model B

The presented halfspace is modified by the BTC element in order to assess the system's response for a bottom layer with a changing water saturation (model B). The results for model A with the WBM and $R = 20$ m are used as reference data and are indicated by a black straight line in Figure 5. For a varying water saturation of the bottom layer, it is assumed that the system's response is located between two limit cases. The first limit case is model A, whereas the second limit case is Model D, which assumes a fully dry elastodynamic halfspace.

Figure 5 illustrates that for a slight change of the saturation from $S = 1.0$ to $S = 0.999$, the computed results start to converge to the response of a dry elastodynamic halfspace. The largest differences are computed for $f = 37.5$ Hz and 50 Hz. They include a maximum decrease in the displacement amplitude of 3.1%. Furthermore, the graph reveals a steady decline of $\overline{u}_y$ for higher excitation frequencies instead of a slight plateau, as shown in section 4.2. This indicates a system behavior, which is more typical for an elastodynamic structure rather than a layered halfspace with a water table. The diagram also includes displacement amplitudes for $S = 0.6$, which indicates that the WBM model continues to approach model D for a decreasing water saturation. However, the most significant system change could be observed for a partial saturation of 0.999.

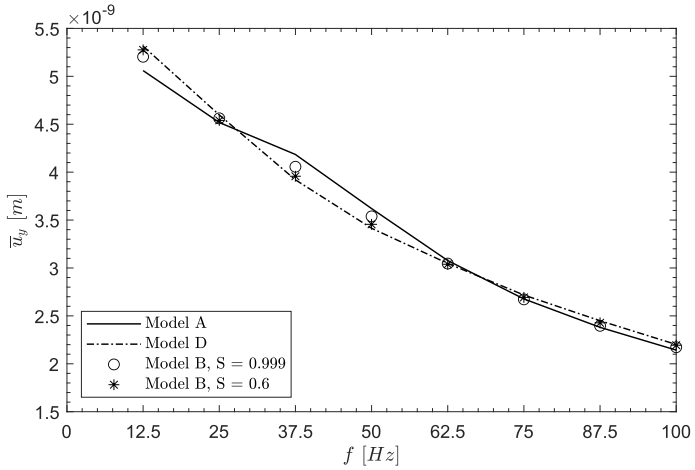

Figure 5: $\overline{u}_y$ for model B and selected degrees of water saturation

This system behavior is related to the computation of the mixed fluid bulk modulus K_f according to the BTC model. For a slight change of the state of full saturation, the bulk modulus of the mixed fluid decreases significantly as the contributions from the water and air phases are involved into a serial connection approach. Figure 6 presents the development of K_f for different degrees of water saturation, which starts at the bulk modulus of air ($S = 0$) and increases until reaching the bulk modulus of water ($S = 1.0$). For $S = 0.999$, the mixed fluid bulk modulus

lies at $2.56 \cdot 10^8$ N/m^2, whereas the bulk moduli for water and air are $K_1 = 2.19996 \cdot 10^9$ N/m^2 and $K_2 = 1.45 \cdot 10^5$ N/m^2. The drop of K_f from $S = 1.0$ to 0.999 causes a significant change in the first P-wave velocity as presented by Figure 7. For $S \to 1.0$, the value of c_{p_1} is closer to the wave speed of a fully dry elastodynamic medium than a fully saturated poroelastic structure.

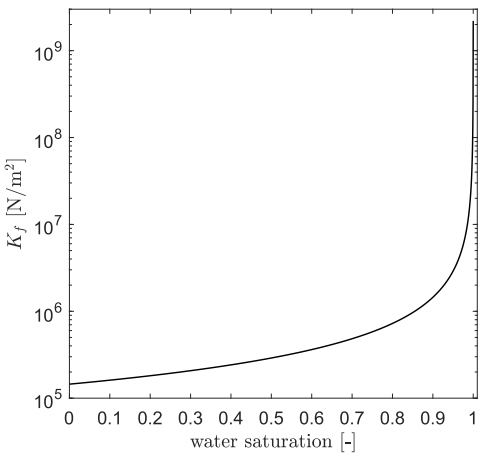

Figure 6: K_f for different degrees of water saturation

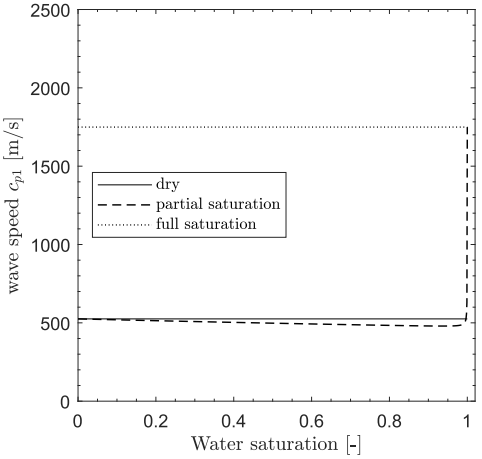

Figure 7: Wave speed for the 1st P-wave ($f = 12.5$ Hz)

4.4 Mean displacement amplitude for model C

In the following example, model A is compared with model C, which assumes an additional water content in the top layer. In order to assess the numerical results, which were achieved with the BTC model for the top layer, two limit cases are considered. The first limit case assumes a fully saturated halfspace according to Biot's theory (model E), whereas the second limit case is a two layered halfspace with fully saturated bottom layer and dry elastodynamic top layer (model A). Figure 8 illustrates the results for model A, model E and model C.

It can been seen that for a slight water saturation of $S = 0.01$, model C delivers displacement amplitudes which are nearly the same as for model A. For higher degrees of saturation as for example $S = 0.5$, the displacement amplitudes for model C become slightly lower and there lies a maximum deviation of -4.0% for $f = 37.5$ Hz. By increasing the degree of saturation to $S = 0.999$, $\overline{u}_y$ of model C approaches the graph of a fully saturated halfspace (model E) as long as $f \leq 50$ Hz. For higher excitation frequencies, the displacement amplitudes tend to the results according to model A. This indicates that the original plateau of the graph $\overline{u}_y$ for $S = 0$ has moved to a higher frequency range. Due to the chosen saturation of $S = 0.999$ and a medium hydraulic conductivity, the top layer tends to the state of a frozen mixture. This means that relative displacements between solid phase and mixed fluid are possible but very small. Consequently, the top layer behaves more like an elastodynamic structure than a saturated medium with loose coupling. As indicated by [16], the amplification of $\overline{u}_y$ due a water table is connected to resonance effects in the top layer. By increasing the saturation to $S = 0.999$, the top layer becomes stiffer and its eigenfrequencies will rise. This causes a shift of the plateau in

the $\overline{u}_y$ graph to a higher frequency range, which means that amplifications of the displacement amplitudes due to layering become relevant for higher excitation frequencies.

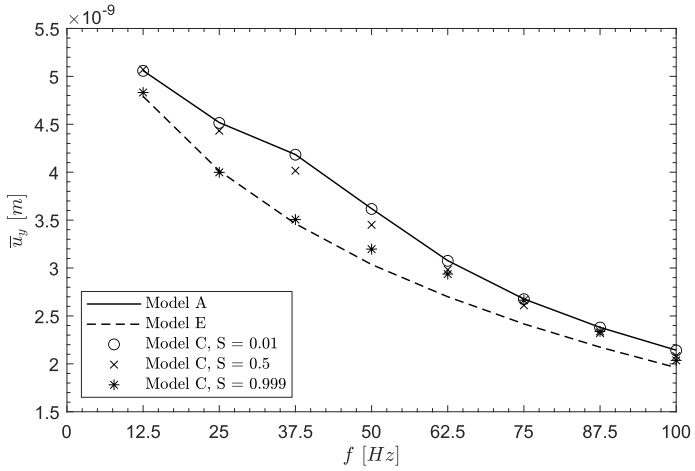

Figure 8: $\overline{u}_y$ for model C and selected degrees of water saturation

5 CONCLUSION

In order to model a layered halfspace with a water table and soil layers with a varying degree of water saturation, the WBM has been applied. In the first step, a halfspace with a dry elastodynamic soil layer and a fully saturated bottom layer was modeled to compute the mean vertical displacement amplitude under a linearly distributed loading. These results were used to compare them with reference solutions from literature. Afterwards, the top and the bottom layer were tested for different degrees of water saturation S by applying the BTC model. According to it, the enclosed air and water phases within the pores of a solid skeleton are described as one mixed fluid. This permits to use Biot's theory for fully saturated poroelastic structures, in order to describe the system's behavior by two irrotational potentials and one solenoidal potential. Otherwise it would be necessary to implement a third P-wave. The fully saturated bottom layer of the original halfspace was modified by an additional air content within the pores and the displacement amplitude was computed for different excitation frequencies. It could be shown that already a slight change from $S = 1.0$ to $S = 0.999$ decreases the displacement amplification effect due to a water table, as less reflections occur along the transition between top and bottom layer. In order to have a similar system behavior for a partially saturated top layer and fully saturated bottom layer, the degree of saturation must be close to 1.0 in the top layer.

REFERENCES

[1] Biot, M. A. Theory of propagation of elastic waves in a fluid-saturated porous solid. I. Low-frequency range. *J. Acoust. Soc. Am.* (1956) **28**(2):168-78.

[2] Biot, M. A. Mechanics of deformation and acoustic propagation in porous media. *J. Appl. Phys.* (1962) **33**(4):1482-98.

[3] Murphy, W. F. Effects of partial water saturation on attenuation in Massilon sandstone and Vycor porous glass. *J. Acoust. Soc. Am.* (1982) **71**(6):1458-1468.

[4] Berryman, J. G., Thigpen, L., Chin, R. C. Y. Bulk elastic wave propagation in partially saturated porous solids. *J. Acoust. Soc. Am.* (1988) **84**(1):360-373.

[5] Lo, W.-C., Sposito, G., Majer, E. Low-frequency dilatational wave propagation through unsaturated porous media containing two immiscible fluids. *Transp. Porous Med.* (2007) **68**(1):91-105.

[6] Smeulders, D. M. J. On wave propagation in saturated and partially saturated porous media, PhD Thesis. Technische Universiteit Eindhoven, (1992).

[7] Degrande, G., de Roeck, G., van den Broeck, P., Smeulders, D. Wave propagation in layered dry, saturated and unsaturated poroelastic media. *Int. J. Solids Structures* (1998) **35**(34-35):4753-4778.

[8] Muraleetharan, K. K., Wei, C. Dynamic behaviour of unsaturated porous media: Governing equations using the theory of mixtures with interfaces (TMI). *Int. J. Numer. Anal. Methods Geomech.* (1999) **23**(13):1579-1608.

[9] Wei, C., Muraleetharan, K. K. A continuum theory of porous media saturated by multiple immiscible fluids: I. Linear poroelasticity. *Int. J. Eng. Sci.*(2002) **40**(16):1807-1833.

[10] Toan, C. D. Hybrid-Trefftz finite elements for elastostatic and elastodynamic problems in porous media, PhD Thesis. Universidade Católica Portuguesa, (2013).

[11] Moldovan, I. D., Toan, C. D., de Freitas, J. A. T. Hybrid-Trefftz displacement finite elements for elastic unsaturated soils. *Int. J. Comput. Methods* (2014) **11**(2).

[12] Lo, W.-C., Sposito, G., Majer, E. Immiscible two-phase fluid flows in deformable porous media. *Adv. Water Resour.* (2002) **25**(8-12):1105-1117.

[13] Lo, W.-C., Sposito, G., Majer, E. Wave propagation through elastic porous media containing two immiscible fluids. *Water Resour. Res.* (2005) **41**(2).

[14] Desmet, W. A wave based prediction technique for coupled vibro-acoustic analysis, PhD. thesis 98D12, Faculteit Toegepaste Wetenschappen, Katholieke Universiteit Leuven, (1998).

[15] Deckers, E., Atak, O., Coox, L., D'Amico, R., Devriendt, H., Jonckheere, S., Koo, K., Pluymers, B., Vandepitte, D., Desmet, W. The Wave Based Method: An overview of 15 years of research. *Wave Motion* (2014) **51**(4):550-565.

[16] Degrande, G. A spectral and finite element method for wave propagation in dry and saturated poroelastic media, PhD Thesis. Katholieke Universiteit Leuven, (1992).

[17] Deckers, E. A wave based approach for steady-state Biot models of poroelastic materials, PhD. thesis 2012D12, Faculty of Engineering, Katholieke Universiteit Leuven, (2012).